Chapter 4

Load Voltage-Based MPPT Technique for Standalone PV Systems Using Adaptive Step

4.1 Introduction

In recent years, PV power generation has been widely used because of increased energy demands and limited resources of fossil fuels. PV systems generate cleaner energy and requires less maintenance. However, the efficiency of a PV system depends on weather conditions like temperature and solar insolation [96, 97]. In addition, the nature of load may vary. Thus, to achieve maximum power from the PV system, a time-varying control is required that connects the varying PV source and the varying load. This controller is called MPPT, that ensures the PV system operates at its maximum power point (MPP) regardless of the environmental condition and load variations [23]. Numerous MPPT techniques have been presented in literature to improve the efficiency of PV module by extracting the maximum power [70, 98–100]. Most of the existing MPPT techniques are broadly categorized as two types: (i) based on input parameters and (ii) based on output parameters [3]. The MPPT algorithm, such as perturb and observe (P&O) [101, 102], Hill-climbing (HC) [43, 103], ripple correlation control (RCC) [104], incremental conductance (IncCond) [105], fuzzy logic control (FLC) [106], particle swarm optimization (PSO) [107,108], neural network (NN) [109,110], and sliding mode control (SMC) [111,112] MPPT schemes have been developed by using input parameters V_{pv} (PV voltage) and

I_{pv} (PV current). The P&O and IncCond schemes are frequently used because of their ease of implementation and better efficiency [113]. However, with these schemes, the operating point drifts away from the maximum power point (MPP) for sudden change in insolation [20, 114]. The RCC scheme utilizes the time derivative of the current ripple and the voltage ripple of power converters to find the location of the operating point on the characteristic curve of the PV module. Further, the time derivative of such voltage and current for high frequency converters is difficult to obtain. Other existing MPPT techniques, such as neural network, fuzzy-logic, optimization algorithms, sliding mode control [106–112] have also been developed. However, these techniques are not commonly used because of their complex nature and the requirement of extensive computing.

The MPPT algorithms may also be implemented by utilizing the output parameters, e.g., converter output voltage V_L and/or converter output current I_L [23,115,116]. In [115], an adaptive frequency and variable step-size MPPT controller is designed by utilizing the load current information. In [116], the maximum power is stored into a battery from the photovoltaic array by maximizing the battery charging current. The possibility of utilizing output parameters to achieve maximum power point depends upon the type of load. An analog MPPT for spacecraft within a low earth orbit is presented in [117], which uses both the input and output parameters for designing the MPPT controller. In [118], a load current based hybrid MPPT controller for single-phase grid-tied photovoltaic systems is designed. In this chapter, a MPPT technique is proposed based on a output parameter rather than the input one. The proposed technique shows significant advantages in terms of MPP tracking ability yet being a simple controller. It is observed that, sensing only one load parameter (either voltage or current) is sufficient for MPP tracking. As a result lesser hardware and simple control algorithm required for MPP tacking [23].

In PV systems, different types of converters are used to achieve the maximum power, such as buck [14], boost [15], buck-boost [16], SEPIC converters [20]. The converters are selected based on the PV module voltage and the load voltage [89]. For example, the buck converter is used for the applications where the required load voltage is always less than the PV module voltage. Similarly, the boost converter is applicable for the case when the PV module voltage is lower than the load voltage. On the other hand, the buck-boost converter is required to regulate the PV module voltage. But the conventional buck-boost converter is not suitable for PV systems, due to discontinuous input current. Also,

it has inverted output voltage. A comparison of different types of buck-boost converters is given in [18]. Among these, even though the SEPIC converter has poor efficiency and higher cost, but it still has many advantages over the conventional buck-boost converter like non-inverting output voltage polarity, continuous input current, works as buck-boost converter over wide range and low input current-ripple [20]. It is suitable for either voltage or current applications [90, 91]. The major losses in the DC-DC converters are switching losses in the MOSFET and the diode, copper losses in the inductor windings and inductor core losses. A comparative analysis of all the losses in converters are given in [92]. It can be seen that all the converters mentioned there in [92] have same number of switches, therefore the switching losses will be the same. The losses in the inductors are lower for the SEPIC converter due to the reduced input ripple current that decreases the peak inductor current even though it has two inductors. These properties make SEPIC converter a suitable candidate for PV applications. In this chapter, SEPIC converter is used for implementation of a new MPPT algorithm, which is realized using a single voltage sensor because the voltage sensing is more simpler than the current one. An hall-effect voltage sensor is used for voltage sensing, which has many advantages such as good linearity, lesser temperature drift, excellent accuracy, optimized response time, wide frequency bandwidth, high immunity to external interference and current overload capacity.

In general, an MPPT technique, utilizing only one voltage sensor is more effective in terms of low complexity and reduced cost. Voltage sensing is less costlier than the current one. In [53], an LVB MPPT method with FSS algorithm has been presented. Due to the FSS, the transient state performance is not up to the mark. In this chapter, an adaptive step-size is applied to obtain faster response. In comparison to similar work in [115], the present work considers voltage sensor only and presents an MPPT based on voltage perturbation instead of the current perturbation. Hence, the present MPPT controller is less costlier due to the absence of a current sensor.

4.2 Problem Formulation

In a PV system, the MPP depends on many factors, such as cell temperature, solar insolation, shading condition and ageing of module [119]. If the PV array is connected

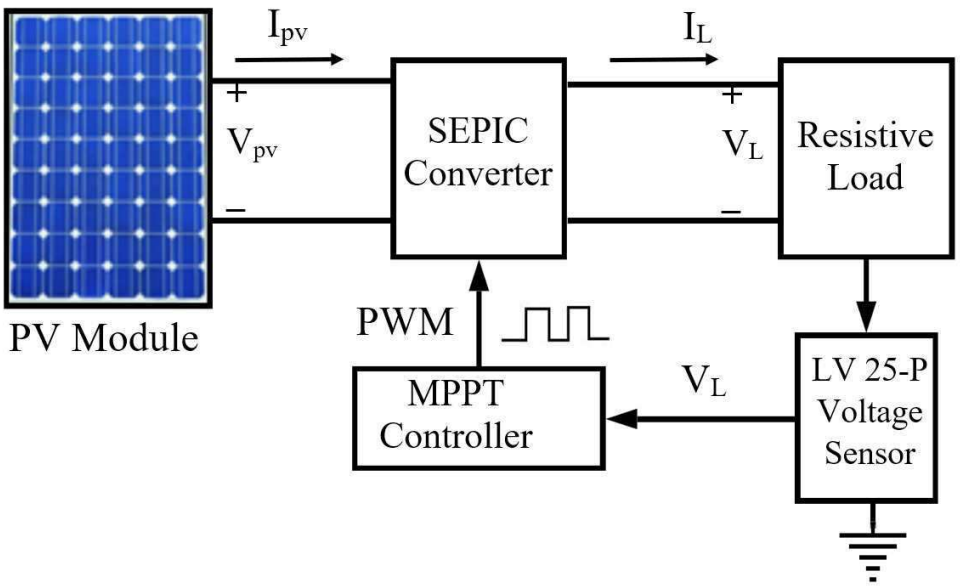

Figure 4.1: Block diagram PV system with MPPT controller.

directly to the load, then MPP operation of the PV system is not ensured. To ensure the PV system operate at MPP, a converter is required to interface the load with the PV system. In this work, SEPIC converter is used as the matching converter by controlling the duty ratio of the converter. The main objective of the control technique is to transfer the maximum available power to the load. This can be achieved either by maximizing the PV power P_{pv} or load power P_L.

In most of the MPPT techniques, maximization of the P_{pv} is done by sensing the input voltage V_{pv} and current I_{pv}. It can be observed that controlling the input power requires sensing of both parameters V_{pv} and I_{pv} regardless of the control algorithm used. For example, in P&O algorithm, the P_{pv} is calculated by multiplying the V_{pv} and I_{pv}, whereas, in IncCond algorithm, V_{pv} and I_{pv} are used for calculation of the incremental and absolute conductance. A comparison of different MPPT techniques, particularly in the perspective of number of sensor used, is given in [3,53,70]. It can be observed that the MPPT techniques based on input parameter requires more number of sensors and more complex as compared to output parameter based MPPT. Also for the output parameter based MPPT controller, only one sensor for sensing I_L or V_L is sufficient [53]. It may be noted that single sensor based MPPT controller can be realized using either input or output parameters of the converter. Taking the output information is always beneficial considering the variable efficiency of the converter at different power level. An output

information based algorithm delivers maximum power to the load instead of maximizing the power extraction from the PV panel using input information.

In most practical PV systems, batteries are used for energy storage, where the converter output voltage and current are already monitored for the protection of the batteries and charge control. Hence, with the same load measurements (V_L & I_L), the PV MPPT control and charge control of batteries can be achieved. As a result, the overall cost of the PV system is reduced. This chapter is based on the utilization of output parameter for achieving maximum power point tracking by using $V_L - D$ characteristic. A block diagram of the considered PV system is shown in Fig. 4.1. A load is connected to the output of the converter and the MPPT controller regulates the duty ratio of the SEPIC converter by sensing only the load voltage V_L.

4.3 Analysis of Load Voltage Based MPPT Technique

In [36], the power derivative with respect to duty ratio dP_{pv}/dD of the PV module is used as a tracking parameter. From the $P_{pv} - D$ waveform shown in Fig. 4.2, it can be seen that the slope $\left(\frac{dP_{pv}}{dD}\right)$ depends on the location of the operating point. It can be written as (4.1),

$$\frac{dP_{pv}}{dD}\begin{cases} = 0, \text{at MPP} \\ > 0, \text{on left of MPP} \\ < 0, \text{on right of MPP} \end{cases} \tag{4.1}$$

For the PV system with resistive load (R_L), PV power (P_{pv}) can be expressed in terms of efficiency (η) by (4.2)

$$P_{pv} = \frac{{V_L}^2}{\eta R_L} \tag{4.2}$$

$$\frac{dP_{pv}}{dD} = \frac{2V_L}{\eta R_L}\frac{dV_L}{dD} \tag{4.3}$$

By considering (4.3), the LVB MPPT technique is developed based on $V_L - D$ waveforms. The relation between converter load voltage V_L with duty ratio D is also shown in Fig.

4.2. The slope $\frac{dV_L}{dD}$ of $V_L - D$ characteristics can be written as (4.4),

$$\left(\frac{dV_L}{dD}\right) \begin{cases} > 0, \text{to the left of MPP} \\ = 0, \text{at MPP} \\ < 0, \text{to the right of MPP} \end{cases} \tag{4.4}$$

Note the similarity of (4.1) and (4.4) that both the slopes are zero at the MPP.

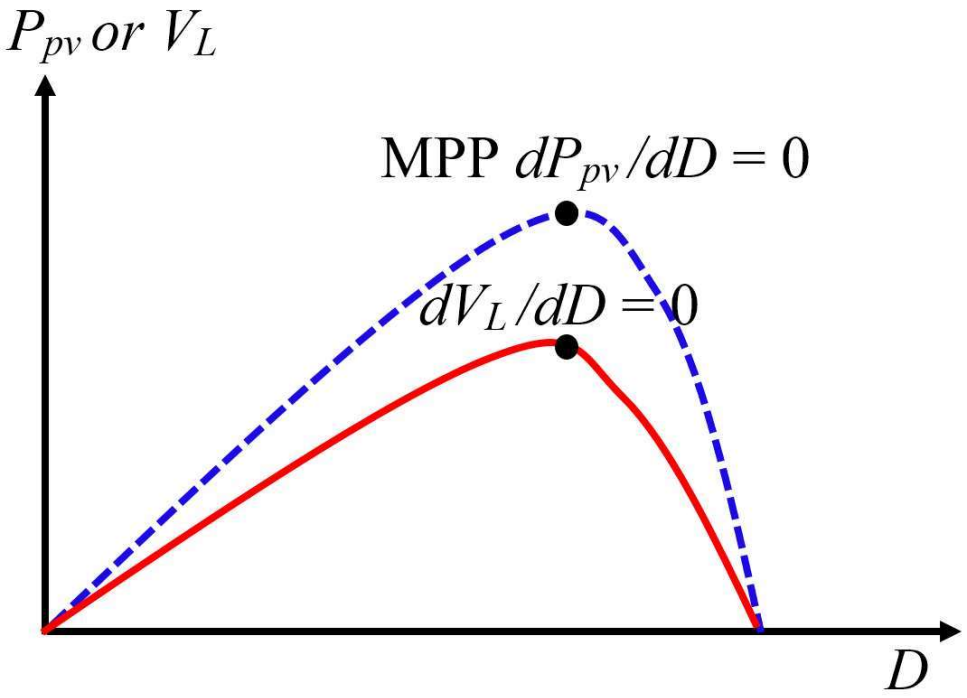

Figure 4.2: Characteristics waveforms of $P_{pv} - D$ and $V_L - D$.

4.4 Proposed Load Voltage Based MPPT Technique

In this section, we propose an MPPT algorithm based on (4.4). A digital implementation of (4.4) is considered for easier computation. This is in contrast to analog MPPT techniques [71, 117, 120] that are complex and demands regular maintenance. However, digital implementation leads to steady-state oscillations around the MPP, which is well known in literature.

For digital implementation, the duty ratio of SEPIC converter and load voltage are represented by $D(i)$ and $V_L(i)$ for present iteration and $D(i-1)$ and $V_L(i-1)$ are for the previous iteration.

A step change in the load voltage and duty ratio from one cycle to the next is defined by

$$dV_L = V_L(i) - V_L(i-1) \tag{4.5}$$

$$dD = D(i) - D(i-1) \tag{4.6}$$

If the slope $\left(\frac{dV_L}{dD}\right)$ is positive, the duty ratio is increased by ΔD (perturbation step-size) and if the slope is negative then the duty ratio is decreased by ΔD.

4.4.1 LVB MPPT Technique with FSS

In [53], the perturbation in duty ratio is done by FSS ΔD (perturbation step-size). However, with the FSS, the MPP tracking time is large at transient-state due to the change in insolation. Because of this, the transient-state efficiency is reduced. To improve the performance of the PV system an ASS scheme is proposed next.

4.4.2 LVB MPPT Technique with ASS

In this chapter, an LVB MPPT with ASS is proposed for reducing the MPP tracking time. The duty ratio value $D(i+1)$ is always varied between minimum value $D_{min} = 0$ and a maximum value $D_{max} = 1$.
Since the proposed MPPT algorithm is considered for digital implementation, the change in duty ratio for next iteration is proposed as:

$$D(i+1) = D(i) \pm \Delta D = D(i) \pm \beta \left| \frac{dV_L}{dD} \right| \tag{4.7}$$

where β is a scaling factor that can be used to scale the ASS in the algorithm.

The ASS MPPT method using load voltage is realized by (4.7). The flowchart of the proposed method is given in Fig. 4.3. It can be observed that the duty ratio perturbation step-size ΔD decreases as the slope $\left(\frac{dV_L}{dD}\right)$ decreases. This indicates that the operating point is approaching towards the MPP. From (4.7), it can be seen that larger value of ΔD at transient-state results in faster tracking speed to the MPP and smaller value of ΔD at steady-state results in lesser oscillation and thereby higher efficiency.

The upper limit of perturbation step-size ΔD_{max} is chosen as 0.05. The lower limit of perturbation step-size ΔD_{min} is set following [115]. For selection of these, the first

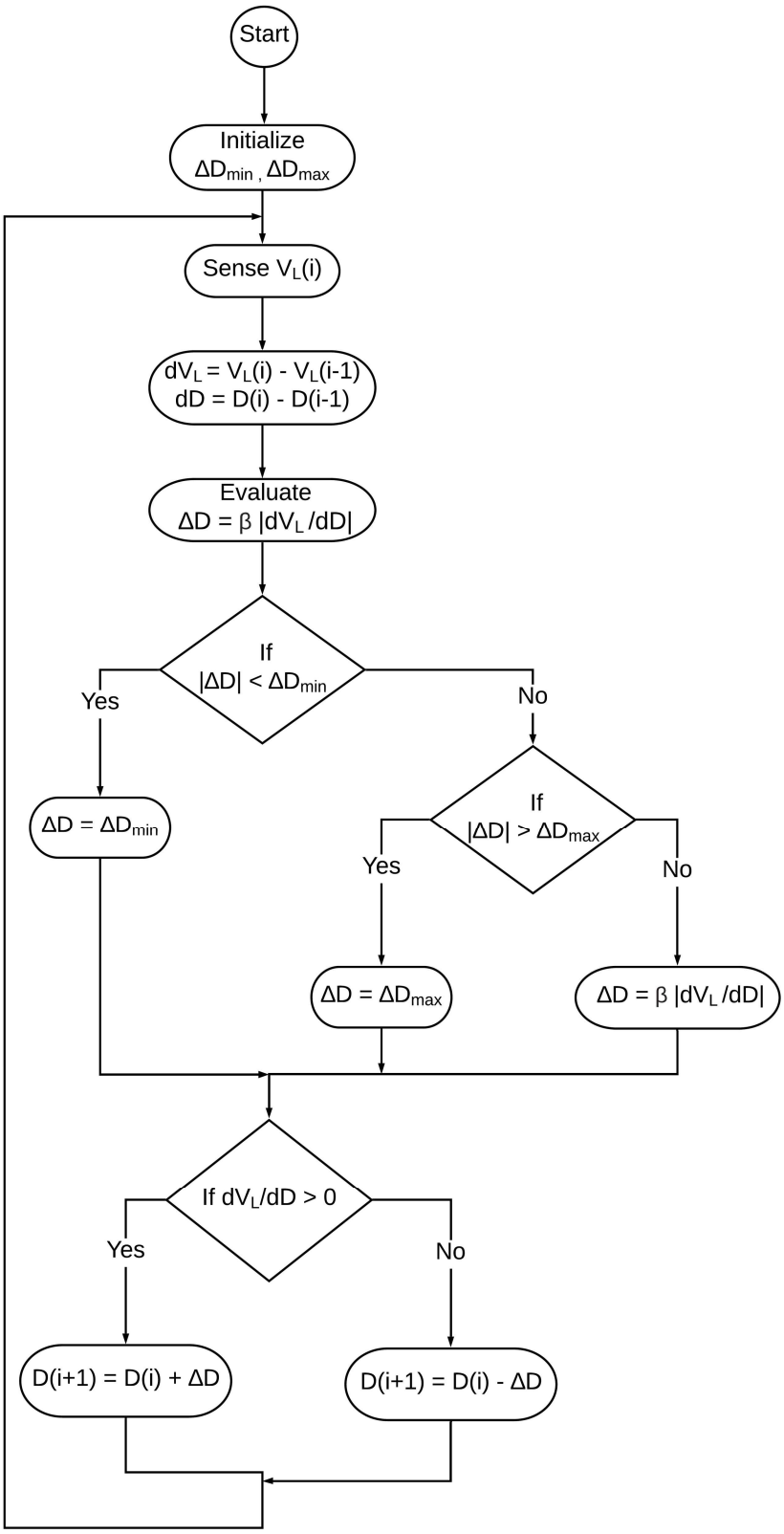

Figure 4.3: Adaptive step-size MPPT algorithm flowchart.

step is to restrict ΔD for tending towards zero, since it will cause the slope $\frac{dV_L}{dD}$ tending towards infinity and the duty ratio D to saturate. The second one is due to the limitation of digital controller hardware resolution (ADC's resolution). For a n-bit ADC, the value of ΔD_{min} is calculated by (4.8)

$$K\left[V(D+\Delta D_{min})-V(D)\right] \geq V_{ADC}/2^n, \tag{4.8}$$

where K is the gain of the voltage sensor and V_{ADC} is maximum voltage of the ADC channel. In this chapter, ΔD_{min} is calculated as 0.005. If the FSS ΔD and the minimum value of the ASS ΔD_{min} are the same, then the steady-state response of both the techniques are same. However, due to ASS, the operating point reaches quickly at steady-state for change in insolation level. This improves the efficiency at transient stage and thereby overall efficiency also improves.

It is required that ΔD has larger value when the operating point is away from the MPP and smaller at steady-state. The scaling factor β can be used for controlling the convergence of the algorithm towards the MPP. A higher value of β leads to faster convergence whereas smaller value leads to slower convergence. However, a large β may lead to larger oscillation around MPP. Since, for a small change in dV_L/dD, large change in ΔD can be seen from (4.7). The value of scaling factor β may be set by (4.9):

$$\frac{\Delta D_{min}}{\left|\frac{dV_L}{dD}\right|_{\Delta D_{min}}} \leq \beta \leq \frac{\Delta D_{max}}{\left|\frac{dV_L}{dD}\right|_{\Delta D_{max}}} \tag{4.9}$$

Similar evaluation has also been given in [115] for determination of such convergence parameter. In this chapter, $\beta = 1$ is chosen to demonstrate the efficacy of the proposed adaptive step-size that can be further improved by choosing a varying β value [94].

4.5 Design and Operation of the SEPIC Converter

The circuit diagram of the SEPIC converter is shown in Fig. 4.4. There are two operating modes of the SEPIC converter: continuous conduction mode (CCM) and discontinuous conduction mode (DCM). To operate it in the CCM mode, the inductor (L_1 and L_2) currents never go to zero before the end of the switching period as shown in Figs 4.5 and 4.6, respectively. CCM operation can be ensured if the value of inductors L_1 and L_2 satisfies the following relation [94]:

$$L_1 = L_2 \geq \frac{V_{pv(min)}}{\Delta I_L \times f_s} \times D_{max} \tag{4.10}$$

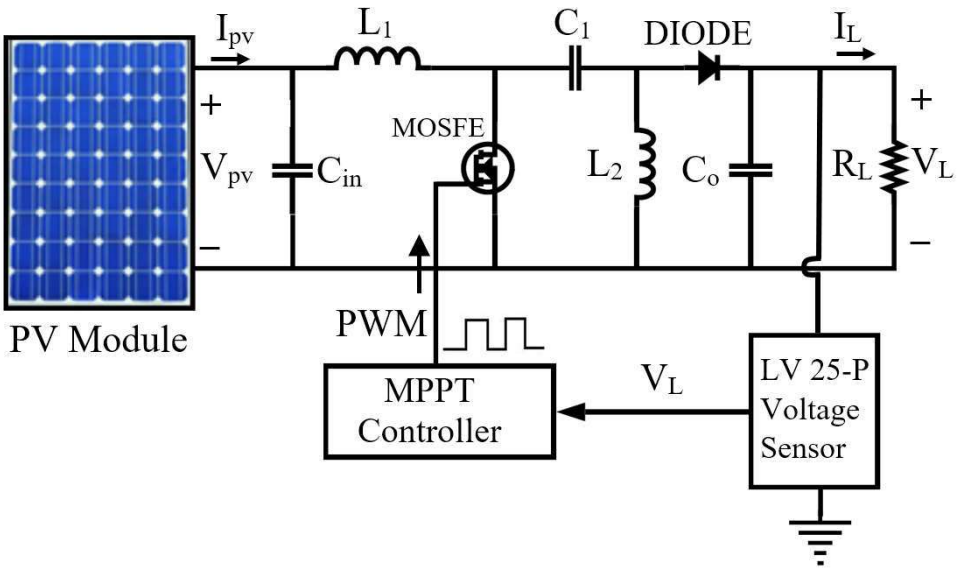

Figure 4.4: Circuit model of developed PV system.

where $V_{pv(min)}$ is minimum input voltage, $\Delta I_L = \Delta i_{L1} = \Delta i_{L2}$ is the ripple current, f_s is the switching frequency and D_{max} is the maximum duty ratio.

In this chapter, the SEPIC converter is designed for a 40 Watt PV module based on the design consideration as the following:
Minimum input voltage $V_{pv(min)} = 8\ V$ and $V_{pv(max)} = 17.4\ V$, output voltage $V_L = 25\ V$, load current $I_L = 1.6\ A$, Switching frequency $f_s = 50\ kHz$ and forward voltage drop across the diode is $V_D = 0.5\ V$.

In practice, the peak to peak ripple current ΔI_L is considered to be 20 to 40 % of the maximum input current $I_{pv(max)}$ at the minimum input voltage $V_{pv(min)}$. Here, the $I_{pv(max)} = 1.8\ A$ is considered. Hence, the ripple current can calculated as:

$$\Delta I_L = \ I_{pv(max)} \times 40\% = 1.8 \times 40\% = 0.72 \tag{4.11}$$

For continuous conduction mode (CCM) operation of the SEPIC converter, the maximum duty-cycle is calculated [95] as:

$$D_{max} = \ \frac{V_L + V_D}{V_{pv(min)} + V_L + V_D} \tag{4.12}$$

By putting all the values in (4.12), one gets

$$D_{max} = \ 0.76 \tag{4.13}$$

Thus the values of inductors L_1 and L_2 are calculated by putting all the values in (4.10). Then, one gets

$$L_1 = L_2 \geq 169\ \mu H \tag{4.14}$$

In this chapter, for CCM mode operation, $L_1 = L_2 = 180\ \mu H$ is selected. Note that, for the chosen input operating range, it will operate in CCM. However, from practical viewpoint, since the input voltage goes even below $8\ V$ in a day of operation, the converter may operate in DCM, though it will operate in CCM in broader operating region.

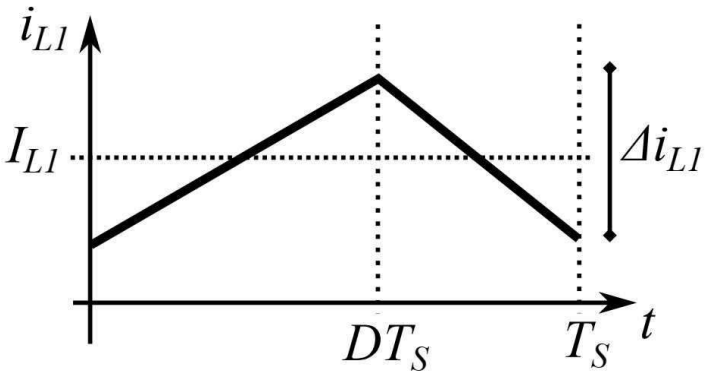

Figure 4.5: Inductor L_1 current waveform.

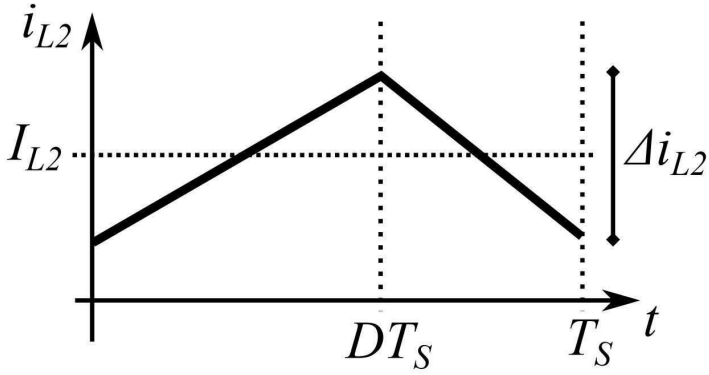

Figure 4.6: Inductor L_2 current waveform.

4.6 Transition Analysis

The $V_L - D$ characteristics of the PV module for three different insolation levels are shown in Fig. 4.7. The insolation levels G_1, G_2 and G_3 are in increasing order. Considering that the present operating point is on the characteristic G_2 and it is at the steady-state, i.e. oscillating around the MPP_2 on the G_2 profile. The average duty ratio at this point corresponds to the MPP_2. Now, if the insolation level increases to G_3, then the operating

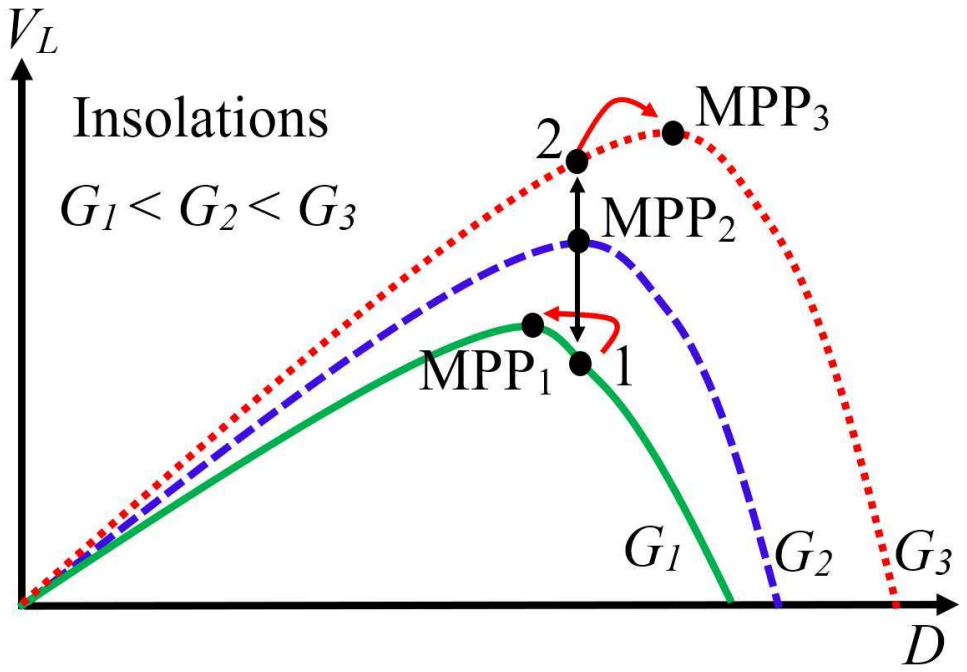

Figure 4.7: $V_L - D$ characteristic at different insolation level.

point moves to a new operating point ② at insolation level G_3. Note that this is not around MPP_3, rather away from it. Also, the slope dV_L/dD is different on either side of the MPP. For increased insolation, the new operating point ② is on the side with smaller slope. Due to smaller slope, the perturbation step-size ΔD is small. Hence the increase in the load voltage for next iteration is smaller. At operating point ②, the algorithm increases the duty ratio, and hence, the operating point moves towards the new maximum power point MPP_3. Similarly for the case of decreased insolation level the operating point moves to new operating point ① on the side with higher slope at insolation level G_2. Due to higher slope, the perturbation step-size ΔD is large and hence a small change in duty ratio causes a sharp decrease in the load voltage. At this operating point, the algorithm decreases the duty ratio, and hence, the operating point moves towards the new maximum power point MPP_1.

4.7 Simulation Results

A single diode model of the PV module from the MATLAB library is used for simulation and its parameters are changed according to PV module ELDROA 40P specifications. The PV module ELDROA 40P in circuit diagram of developed PV system is considered

Table 4.1: Design parameters of SEPIC Converter

Parameters	**Value**
Inductor L_1	180 μH
Inductor L_2	180 μH
Capacitor C_1	47 μF
Input filter Capacitor C_{in}	440 μF
Output filter Capacitor C_o	220 μF
Switching Frequency f_s	50 kHz
Load Resistance R_L	25 Ω

for experimental setup as shown in Fig. 4.4. The specification of this PV module are: $V_{OC} = 21.9\ V$, $I_{SC} = 2.45\ A$, $V_{MPP} = 17.4\ V$ and $I_{MPP} = 2.3\ A$. The SEPIC converter is designed using the design parameter given in Table 4.1.

The proposed MPPT technique has been simulated for a step change in insolation level from 270 W/m^2 to 500 W/m^2 at 1.0 s. The FSS ΔD and the sampling time (T_a) are considered as 0.005 and 27.6 ms, respectively. The proposed LVB MPPT algorithm is applied on the load side, that is automatically doing MPPT at input side of converter. The converter output convergence response and corresponding input tracking waveforms for FSS and ASS are shown in Fig. 4.9 and Fig. 4.10, respectively. The load voltage and the load current are shown in Fig. 4.9 (a) and (b), respectively. Since the proposed technique is based on the load voltage, it is interesting to observe the PV power at the MPP operation. As shown in Fig. 4.10 (a) and (b), the PV voltage and the current also reaches the MPP. It can be seen that a sudden increase in the PV voltage and the PV current for step increase in insolation level from 0 W/m^2 to 270 W/m^2 and 270 W/m^2 to 500 W/m^2. As discussed in section 4.6, the operating point moves to a new operating point on the smaller slope side of $V_L - D$ curve for step increase in insolation level and then it moves towards the new MPP. The Fig. 4.9 (c) shows the load power at output side of SEPIC converter and 4.10 (c) shows the PV power at input side of SEPIC converter and both are taken for the same operating condition. The duty ratio variation for FSS and ASS are shown in Fig. 4.8 (d), which shows that the three level [20] operation of the proposed technique. It can be seen that the change in duty ratio ΔD for the proposed

technique is larger at the transient-state compared to the steady-state. Both the MPPT methods effectively converges to the corresponding MPP voltage and current. But the MPP convergence time is large with the FSS as compared to the ASS. From Fig. 4.10, it can be seen that, the convergence time with FSS for insolation level $G = 270\ W/m^2$ is $T_1 = 276\ ms$, and it is reduced to 110 ms with the help of proposed ASS method. Also, the convergence time reduced to $T_2 = 193\ ms$ from 497 ms for change in insolation from $G = 270\ W/m^2$ to 500 W/m^2.

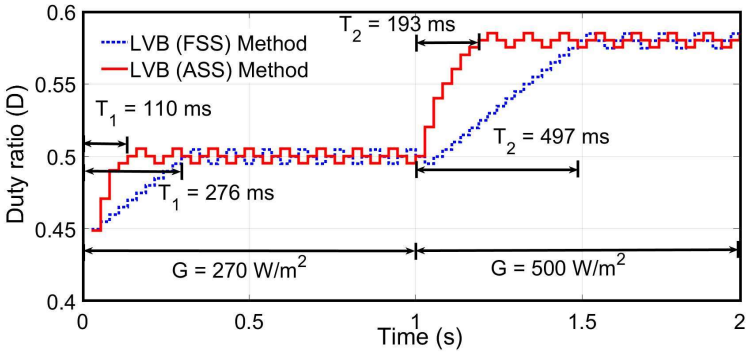

Figure 4.8: Duty-ratio waveform for LVB MPPT method using FSS and ASS for resistive load.

4.7.1 Tracking Efficiency

A comparison of performance in terms of efficiency is presented now. Fig. 4.11 shows tracking responses for the proposed MPPT using ASS, P&O and IncCond methods for step change in insolation levels. The average MPP tracking efficiency $\eta_{MPP(avg)}$ is calculated as [94].

$$\eta_{MPP(avg)} = \frac{P_{MPP(avg)}}{P^*_{MPP(avg)}} \times 100 \tag{4.15}$$

where $P^*_{MPP(avg)}$ is the available average maximum PV power. For insolation level $G = 270W/m^2$, it is 10.51 W. $P_{MPP(avg)}$ is the extracted average maximum power from the PV module. In Fig. 4.11, for the insolation level $G = 270W/m^2$, the PV power reaches steady-state after $t = 0.4\ s$ for all the techniques. So, the average values of extracted maximum PV power $P_{MPP(avg)}$ from PV module is calculated between the time ranges $t = 0\ s$ to 0.4 s and 0.4 s to 1.0 s to make a comparison of transient and steady-state efficiencies. The average tracking efficiency computed for these two time ranges are given in Table 4.2. It can be observed that the average efficiency is improved with the proposed ASS LVB

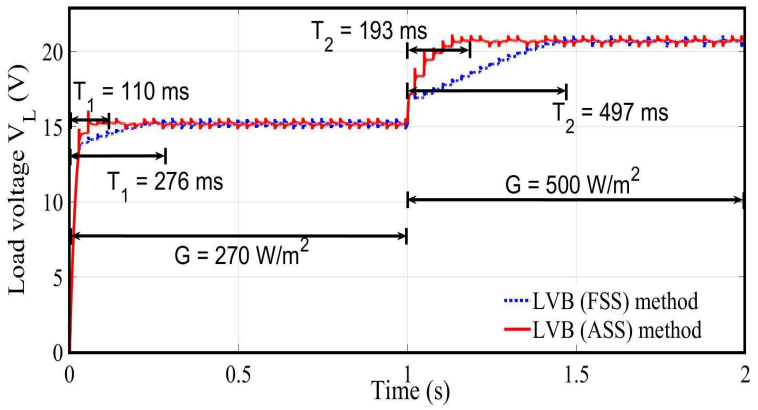

(a)

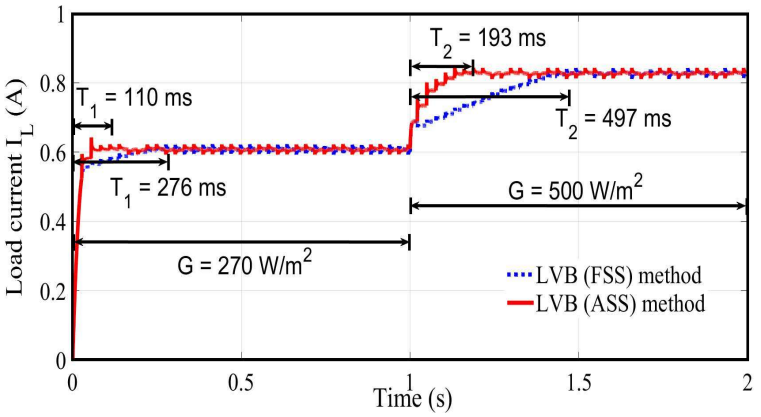

(b)

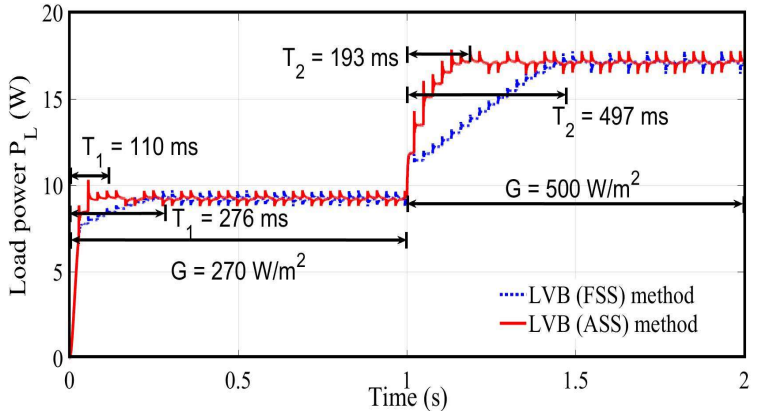

(c)

Figure 4.9: Converter output convergence responses with LVB MPPT method using FSS and ASS for resistive load (a) Load Voltage (V_L) (b) Load Current (I_L) (c) Load Power (P_L).

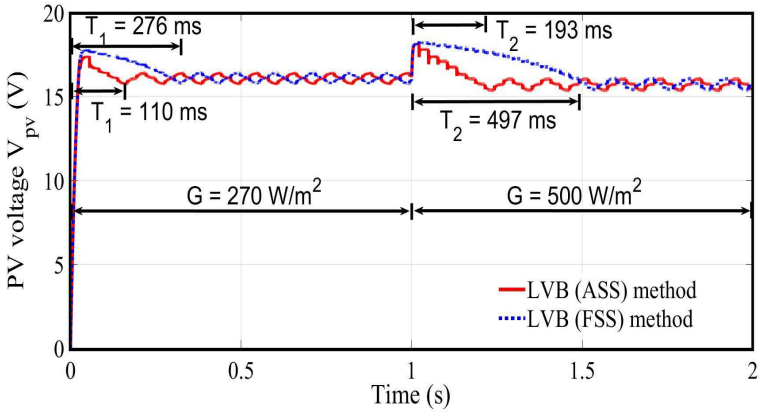

(a)

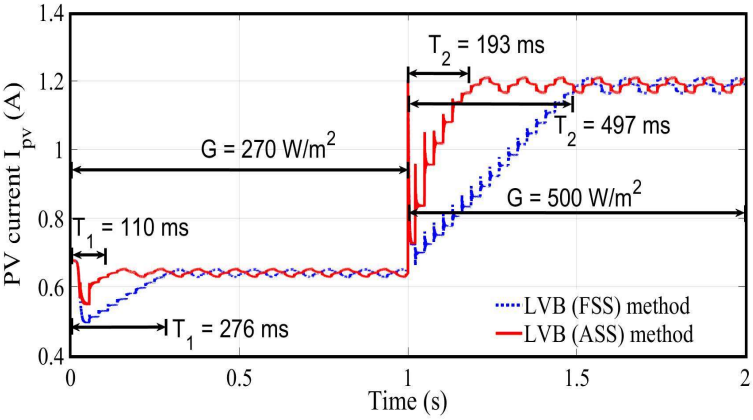

(b)

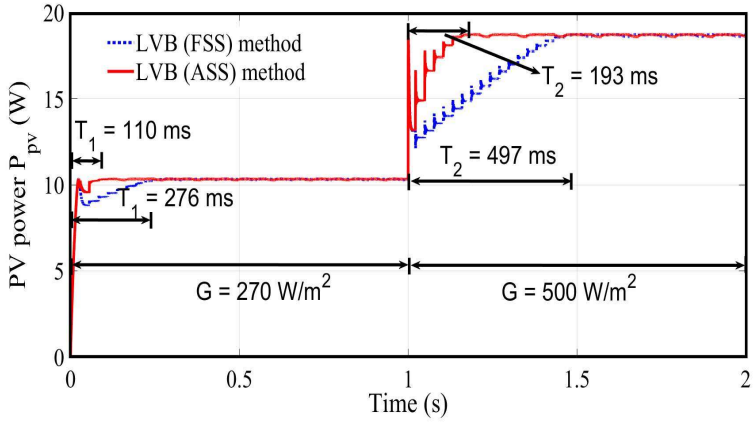

(c)

Figure 4.10: Converter input convergence responses with LVB MPPT method using FSS and ASS for resistive load (a) PV Voltage (V_{pv}) (b) PV Current (I_{pv}) (c) PV Power (P_{pv}).

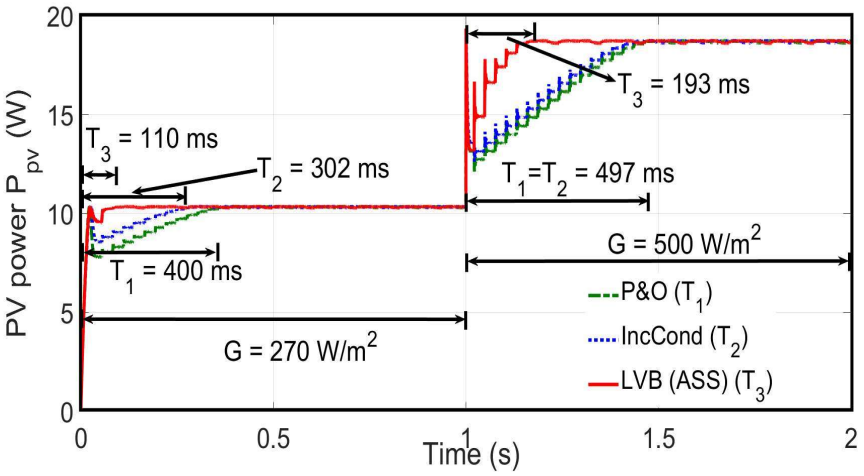

Figure 4.11: Comparison of proposed LVB (ASS) MPPT method with P&O. and IncCond method.

technique considerably during the transient-state due to the improved convergence time though average efficiency at steady-state is almost similar to the other methods since the ΔD_{min} is considered to be the same for all the methods.

Table 4.2: Comparison of simulation results of MPPT techniques

Parameters	**P&O**	**IncCond**	**LVB (ASS)**
$P_{MPP(avg)}$ (W) (0 - 0.4 s)	8.9447	9.3050	10.0374
$\eta_{MPP(avg)}$ (0 - 0.4 s)	85.11 %	88.53 %	95.50 %
$P_{MPP(avg)}$ (W) (0.4 s - 1 s)	10.3084	10.3171	10.3213
$\eta_{MPP(avg)}$ (0.4 s - 1 s)	98.08 %	98.16 %	98.20 %

4.7.2 Ropp Test

The proposed MPPT techniques also tested for Ropp profile [121, 122] of insolation level. The Ropp profile of insolation level is shown in Fig. 4.12 with fast, slow and sudden change in insolation-levels. The convergence response of the PV power with LVB technique using fixed and adaptive step-size is shown in Fig. 4.13. Note that such an Ropp profile emulates different operating points including the time varying one. The proposed techniques performs well for such variations in the insolation as well. The tracking response for ramp and step changes are much better for LVB ASS method than the FSS

method.

4.8 Hardware Implementation and Experimental Results Validation

A solar PV system prototype is developed in the laboratory as shown in Fig. 4.14 to validate the functionality and convergence performance of the proposed LVB MPPT algorithms. A SEPIC converter is designed based on the specifications given in Table 4.1. To implement the proposed technique and generate the desired PWM control signal for the SEPIC converter, an ARDUINO UNO microcontroller is used. The converter voltage and current are measured by LEM LV 25-P and LTS6-NP hall effect sensor, respectively. To generate the artificial insolation, halogen lamps and bulbs are used. The insolation of light is controlled by manual ON-OFF switches and the insolation is measured by using the solar power meter WACO 206.

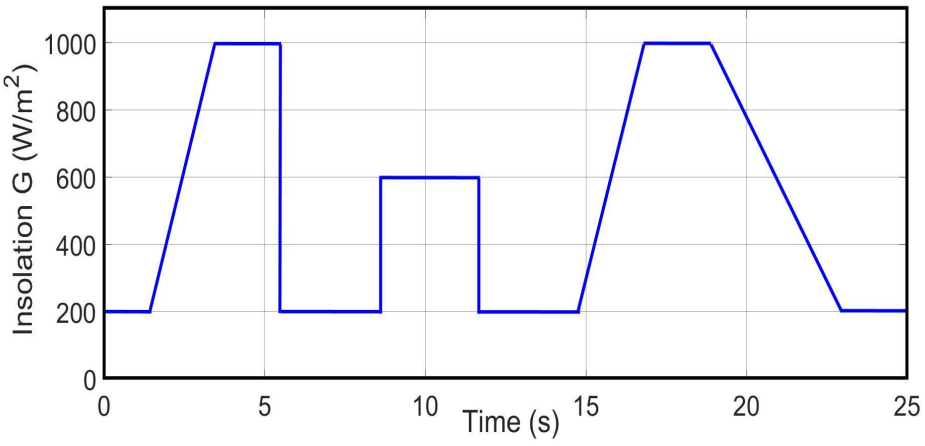

Figure 4.12: Ropp profile of insolation-level.

The LVB MPPT algorithm with fixed and adaptive step-size are compared for the change in solar insolation. The FSS with $\Delta D = 0.005$ and sampling time $T_s = 27.6$ ms are considered for experimental validation. The converter output responses for both fixed and adaptive step-size methods are shown in Fig. 4.15 and 4.16, respectively. The converter input responses for both the FSS and the ASS methods are given in Fig. 4.17 and 4.18, respectively. From Fig. 4.17 (a) and 4.18 (a), it can be observed that the MPP convergence time with FSS is $T_1 = 3200$ ms, and it is reduced to 1200 ms with ASS at

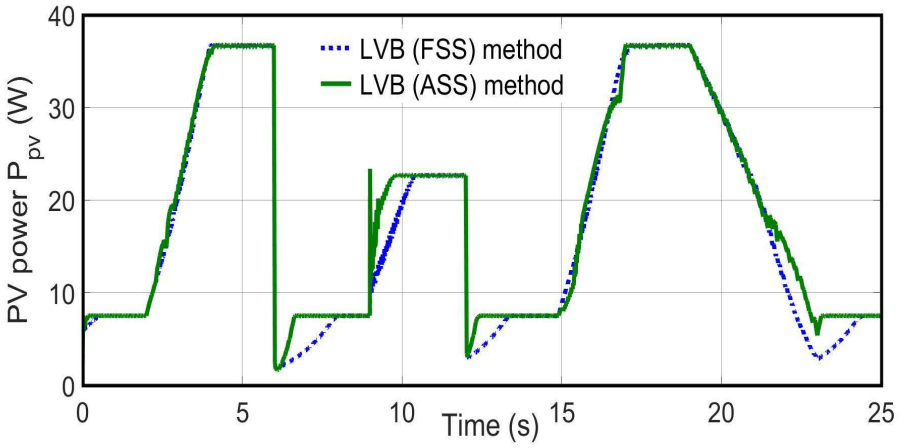

Figure 4.13: PV power P_{pv} with LVB MPPT method using FSS and ASS.

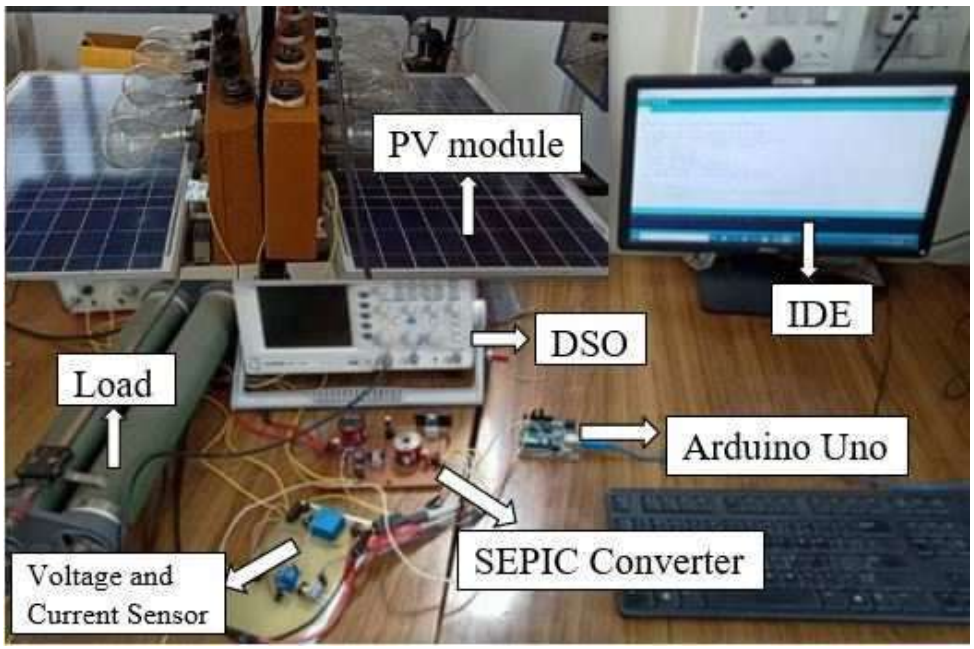

Figure 4.14: Developed hardware setup of PV system for experimental validation.

insolation level $G = 270\ W/m^2$. The MPP convergence time $T_2 = 2400\ ms$ is reduced to 1200 ms, when the insolation is increased form 270 W/m^2 to 500 W/m^2 as shown in Fig. 4.17 (b) and 4.18 (b). The convergence time $T_3 = 2000\ ms$ is reduced to 1000 ms with ASS for decrease in insolation from 500 W/m^2 to 270 W/m^2 as shown in Fig. 4.17 (c) and 4.18 (c).

Following the discussion in section 4.6, for the case when insolation level increases from $G = 270\ W/m^2$ to $G = 500\ W/m^2$, the operating point moves to a new operating point on smaller slope side at $G = 500\ W/m^2$ insolation curve. Due to the smaller slope, the increment in the load voltage and the current for the next iterations are smaller as seen in Fig. 4.15 (b) and 4.16 (b). Similarly, for case when the insolation level decreases from $G = 500\ W/m^2$ to $G = 270\ W/m^2$, the operating point moves to a new operating point located below on the higher slope side of the $G = 270\ W/m^2$ insolation level curve. The voltage drop can be observed in Fig. 4.15 (c) and 4.16 (c) and thereafter the voltage increases to reach the MPP. Due to this reason, the undershoot in the case of decrease in insolation occurs.

The experimental convergence responses of P&O and IncCond methods at insolation level $G = 270\ W/m^2$ are given in Fig. 4.19 and 4.20, respectively. It can be seen that the MPP convergence time for P&O is 5300 ms and for IncCond is 4500 ms, which is quite larger than the proposed MPPT technique. A comparison of MPP convergence times for step change 0 to 270 W/m^2 of the MPPT methods are shown in Table 4.3.

The average values of tracking efficiency $\eta_{MPP(avg)}$ of the experimental results for change in insolation-level form 0 to 270 W/m^2 are calculated based on (4.15), where the value of $P^*_{MPP(avg)}$ is 10.51 W. The average tracking efficiencies are approximately same for both the input side and output side convergence response because the MPP tracking time is same on both the sides, hence input side convergence response is considered for calculation. From Figs. 4.17 (a), 4.18 (a), 4.19 and 4.20, it can be observed that all the responses are reach at steady-state after 5300 ms. Hence the average extracted powers and efficiencies are calculated for two time ranges, one for 0 to 5.3 s and the other for 5.3 s to 10 s, to differentiate the transient and steady-state efficiencies as shown in Table 4.3. It can be observed that the tracking efficiency $\eta_{MPP(avg)}$ is considerably improved with proposed LVB MPPT techniques using adaptive step-size during both the transient as well as steady-state as compared to P&O and IncCond techniques.

Table 4.3: Comparison of experimental results of MPPT techniques

Parameters	**P&O**	**IncCond**	**LVB (ASS)**
Convergence time	5300 ms	4500 ms	1200 ms
$P_{MPP(avg)}$ (W) (0 - 5.3 s)	7.6214	7.9742	9.2879
$\eta_{MPP(avg)}$ (0 - 5.3 s)	72.51 %	75.87 %	88.37 %
$P_{MPP(avg)}$ (W) (5.3 s - 10 s)	9.6475	9.6523	9.6735
$\eta_{MPP(avg)}$ (5.3 s - 10 s)	91.79 %	91.83 %	92.04 %

Overall conclusion and comprehensive discussion on thesis work is discussed in chapter 5.

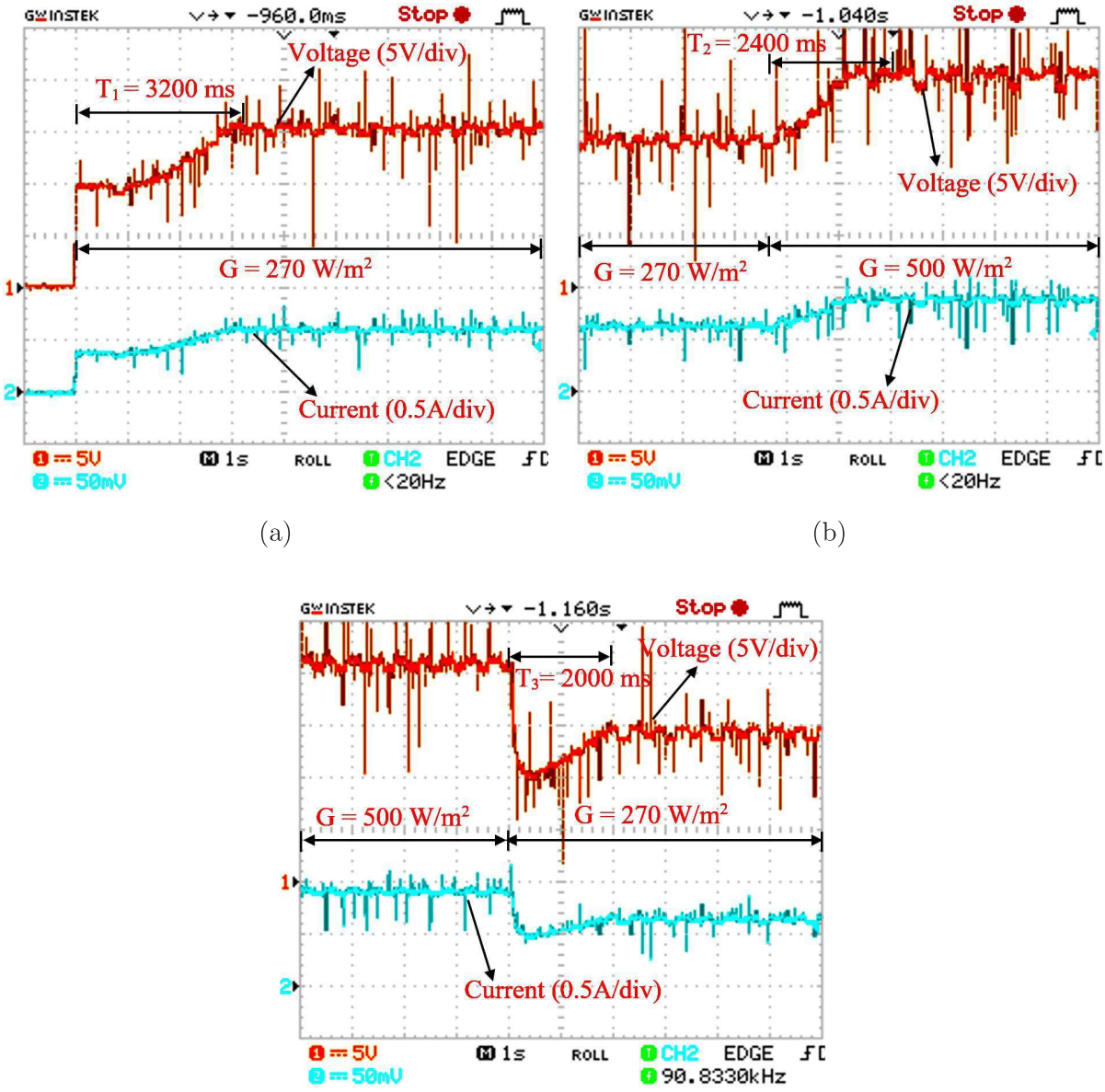

(a) (b)

(c)

Figure 4.15: Load voltage (V_L) and load current (I_L) convergence responses with FSS method (a) start-up for G = 270 W/m^2 (b) for change in insolation from G = 270 W/m^2 to 500 W/m^2 (c) for change in insolation from G = 500 W/m^2 to 270 W/m^2.

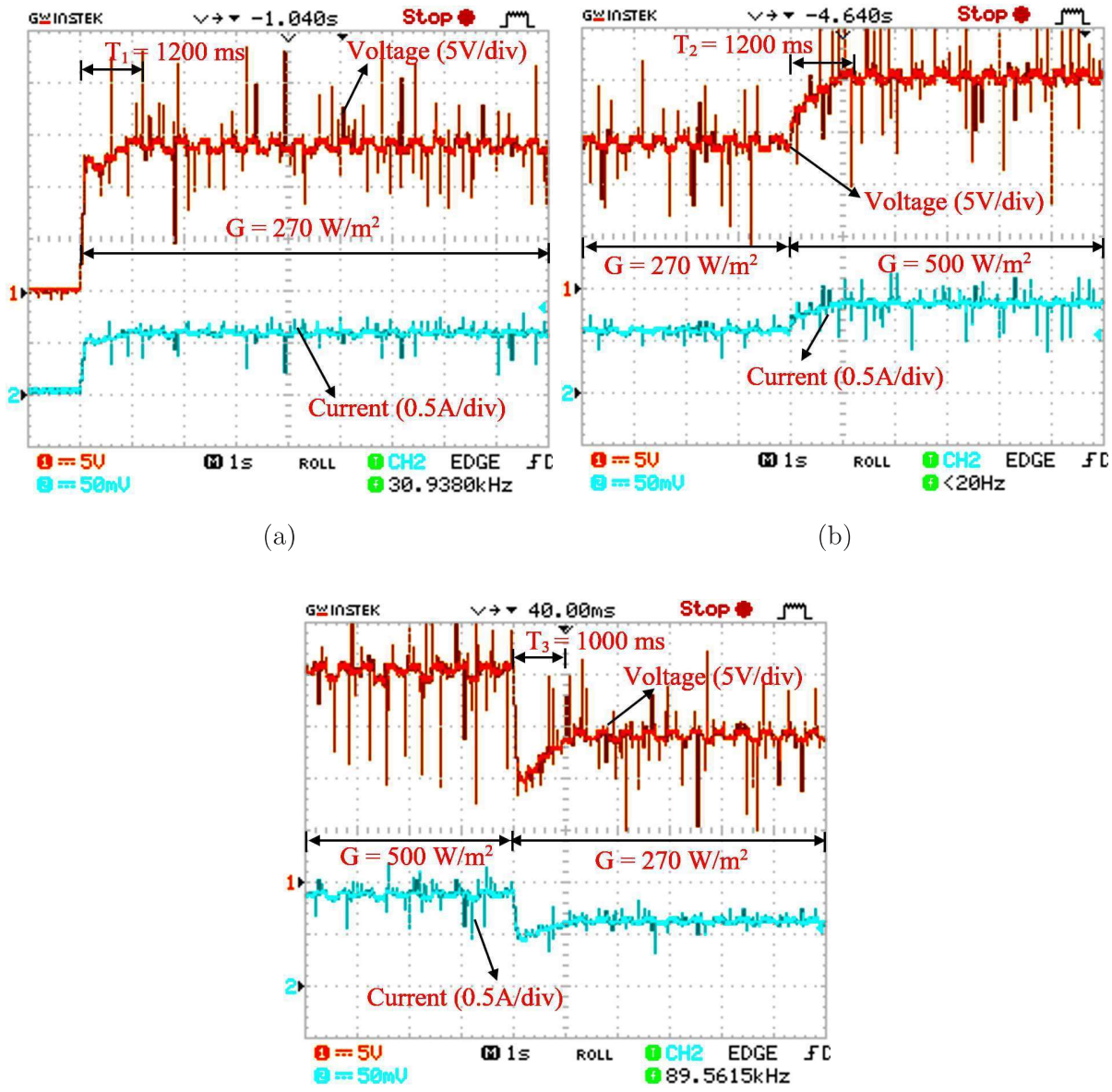

(a) (b)

(c)

Figure 4.16: Load voltage (V_L) and load current (I_L) convergence responses with ASS method (a) start-up for G = 270 W/m^2 (b) for change in insolation from G = 270 W/m^2 to 500 W/m^2 (c) for change in insolation from G = 500 W/m^2 to 270 W/m^2.

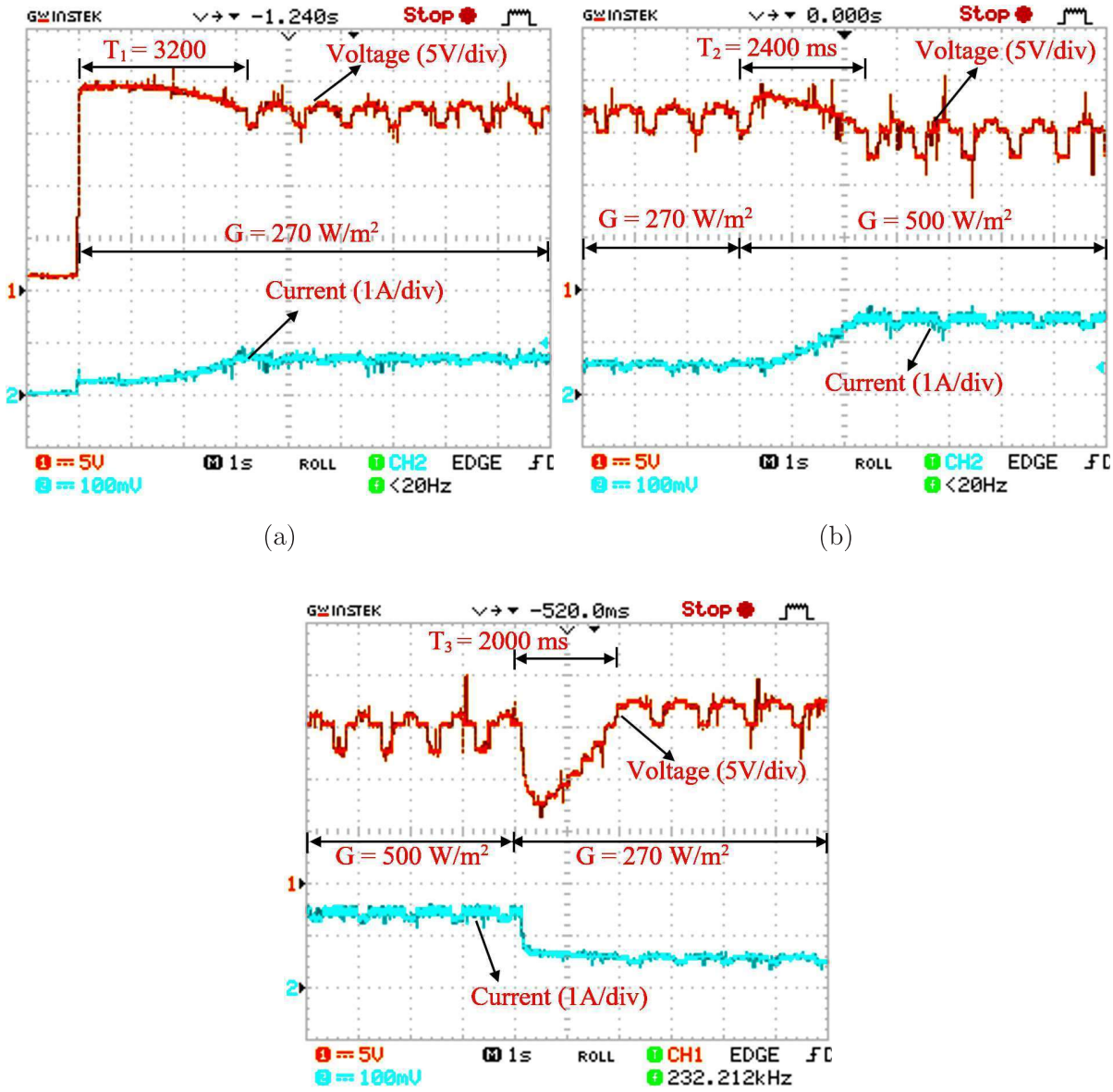

Figure 4.17: PV voltage (V_{pv}) and PV current (I_{pv}) convergence responses with FSS method (a) start-up for G = 270 W/m^2 (b) for change in insolation from G = 270 W/m^2 to 500 W/m^2 (c) for change in insolation from G = 500 W/m^2 to 270 W/m^2.

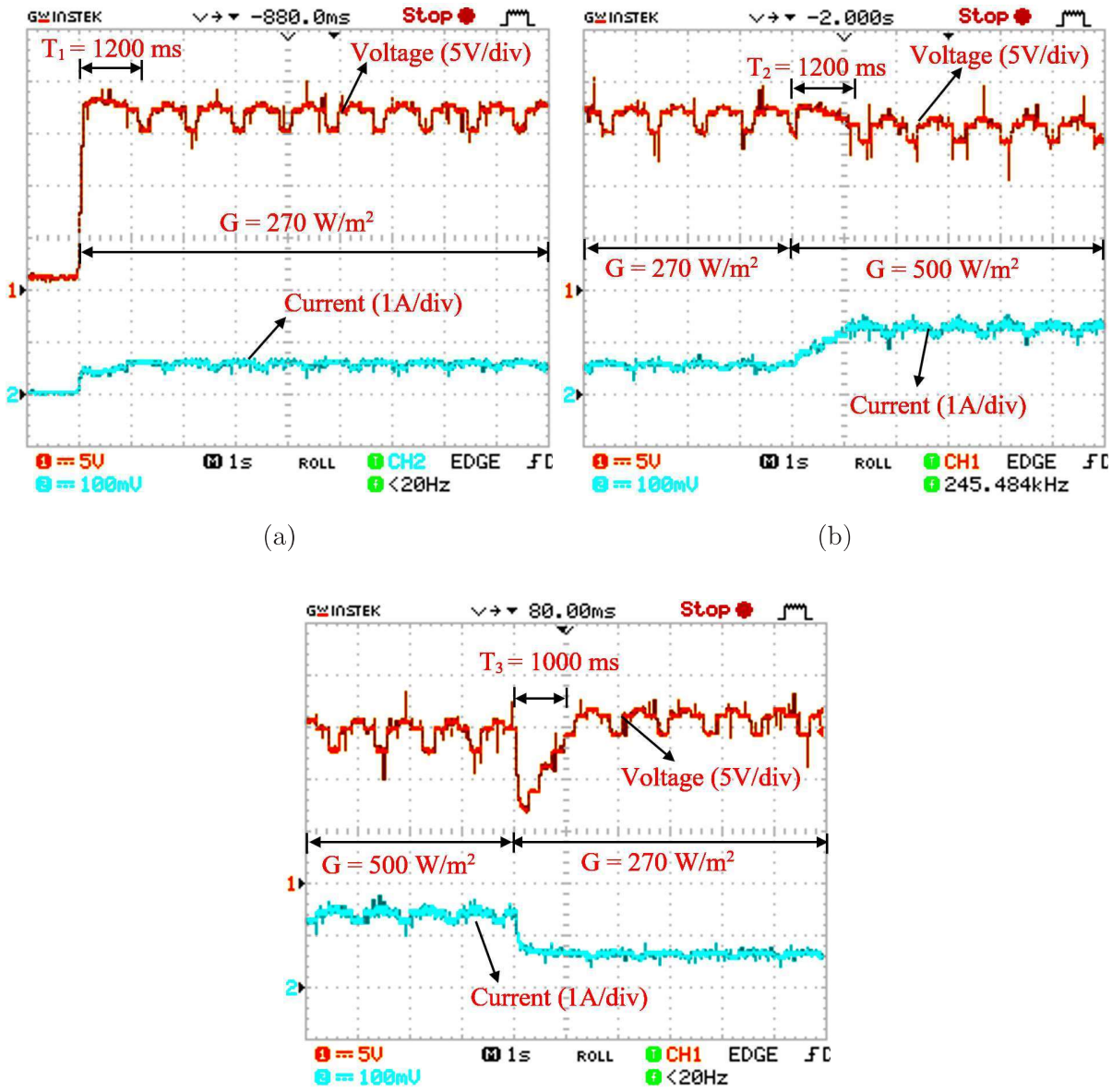

(a) (b)

(c)

Figure 4.18: PV voltage (V_{pv}) and PV current (I_{pv}) convergence responses with ASS method (a) start-up for G = 270 W/m^2 (b) for change in insolation from G = 270 W/m^2 to 500 W/m^2 (c) for change in insolation from G = 500 W/m^2 to 270 W/m^2.

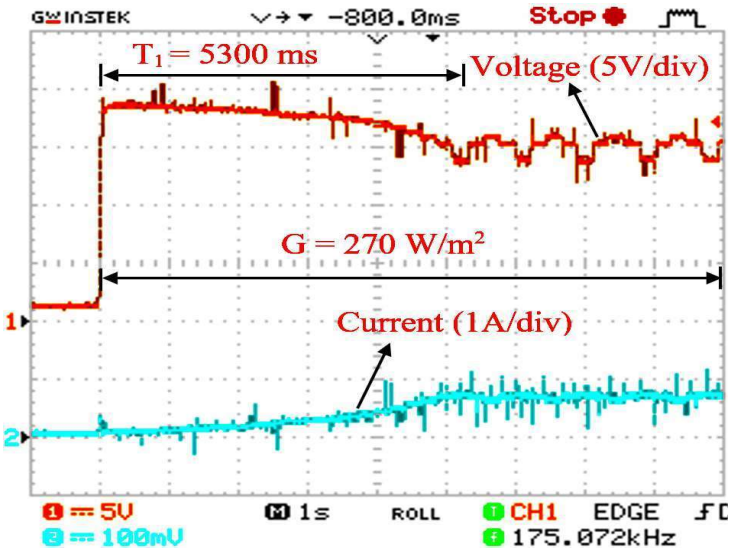

Figure 4.19: Convergence response of PV voltage (V_{pv}) and PV current (I_{pv}) using fixed step-size at G = 270 W/m^2 for P&O algorithm.

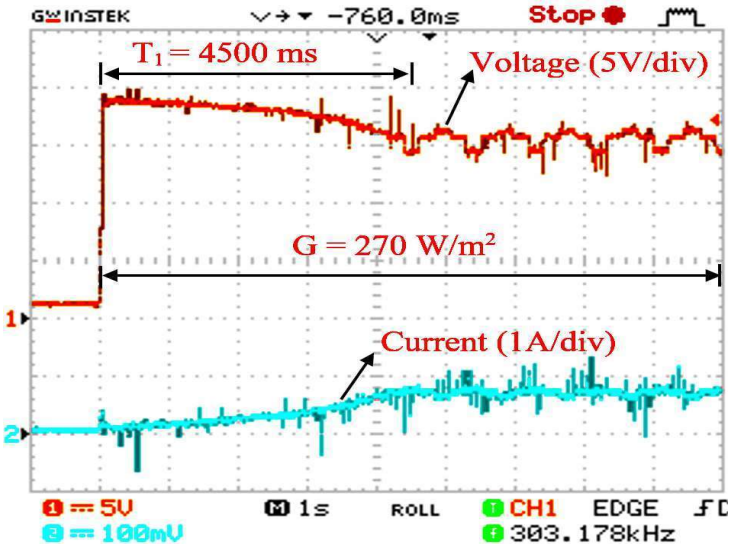

Figure 4.20: Convergence response of PV voltage (V_{pv}) and PV current (I_{pv}) using fixed step-size at G = 270 W/m^2 for IncCond algorithm.